Journal of the European Ceramic Society **10** (1992) 151–159

SiC and Si_3N_4 Materials with Improved Fracture Resistance

H.-J. Kleebe

Max-Planck-Institut für Metallforschung, Institut für Werkstoffwissenschaft, Seestraße 92, D-7000 Stuttgart 1, Germany

(Received 12 February 1992; accepted 24 April 1992)

Abstract

The SiC and Si_3N_4 materials studied were densified to near theoretical density via liquid-phase sintering. All materials have been investigated by means of transmission electron microscopy (TEM). The observed characteristic microstructural features were correlated to fracture resistance. Toughness measurements were performed using the chevron notch configuration. Both SiC and Si_3N_4 materials showed an improved fracture resistance compared with commercially available grades. The toughness values obtained from load/displacement records were 6–7 $MPa\sqrt{m}$ for SiC and 9–11 $MPa\sqrt{m}$ for the Si_3N_4 grades. Additional high-resolution and analytical electron microscopy studies (HREM and AEM) were performed to relate characteristic interfacial features to the resulting mechanical properties. TEM observations revealed marked differences between the two non-oxide ceramic materials analyzed. The major difference regarding the overall microstructures of SiC and Si_3N_4 is twofold: (i) SiC shows matrix grains with a more globular morphology, while in Si_3N_4 large elongated grains are present with a grain diameter of up to 3 μm and a length of ≥ 30 μm; (ii) no amorphous intergranular films were observed in the SiC material with improved toughness, while in Si_3N_4 materials thin amorphous grain- and phase-boundary films were always present. From HREM observations it can be concluded that the presence or absence of amorphous intergranular films governs the resulting fracture resistance and the overall toughening mechanism.

Flüssigphasensinterung der untersuchten SiC and Si_3N_4 Materialien führte zu nahezu vollständiger Verdichtung. Transmissionselektronenmikroskopie (TEM) diente der Materialcharakterisierung. Die charakteristischen Gefügemerkmale wurden mit den ermittelten Bruchzähigkeitsdaten (Chevron-Notch Konfiguration) korreliert. Die SiC und Si_3N_4 Materialien zeigten eine deutliche Bruchzähigkeitssteigerung verglichen mit kommerziellen Materialien. Last/Dehnungskurven lieferten Zähigkeitswerte von 6–7 $MPa\sqrt{m}$ für SiC und 9–11 $MPa\sqrt{m}$ für Si_3N_4. Hochauflösende und analytische Elektronenmikroskopie (HREM und AEM) wurden zusätzlich eingesetzt, um spezifische Grenzflächenstrukturen den resultierenden mechanischen Eigenschaften zuzuordnen. Die TEM Beobachtungen zeigten wesentliche Unterschiede in der generellen Gefügeausbildung der beiden nicht-oxidischen Materialien: (i) die SiC Matrixkörner sind im Vergleich zu den großen, langgestreckten Si_3N_4 Partikeln, die einen Durchmesser von 3 μm und eine Länge von ≥ 30 μm aufweisen, eher globular ausgebildet; (ii) im SiC Material mit erhöhter Bruchzähigkeit wurden keine amorphen Korngrenzfilme beobachtet, wohingegen die Si_3N_4 Materialien stets amorphe Korngrenzfilme entlang von Korn- und Phasengrenzen aufweisen. Die HREM Untersuchungen lassen den eindeutigen Schluß zu, daß das Auftreten bzw. die Abwesenheit amorpher Korngrenzfilme die resultierende Bruchzähigkeit sowie den zähigkeitssteigernden Mechanismus bestimmen.

Des matériaux en SiC et en Si_3N_4 ont été frittés en présence d'une phase liquide jusqu'à une densité proche de la densité théorique. Ils ont été étudiés par microscopie électronique à transmission (MET). Les caractéristiques microstructurales observées ont été corrélées à la résistance à la rupture. Les ténacités ont été mesurées par entaille chevron. Les 2 matériaux (SiC et Si_3N_4) présentent une meilleure résistance à la rupture que leurs équivalents commerciaux.

Les valeurs de la ténacité déduites des enregistrements du diagramme charge/déplacement étaient de 6

Journal of the European Ceramic Society 0955-2219/92/$5.00

à 7 MPa $\sqrt{m}$ pour le SiC et de 9 à 11 MPa $\sqrt{m}$ pour le Si_3N_4.

Des études supplémentaires en microscopie électronique à haute résolution (MEHR) et en microanalyse électronique (MAE) ont permis d'établir la relation entre les particularités de leurs caractéristiques interfaciales et leurs propriétés mécaniques. Les observations au MET ont montré des différences importantes entre les 2 céramiques non-oxyde étudiées. Les différences essentielles des microstructures du SiC et du Si_3N_4 considérées dans leur ensemble sont doubles.

1. SiC présente une structure constituée de grains de morphologie plus globulaire, au contraire de Si_3N_4, où des grains allongés de grandes dimensions sont observés (diamètres jusqu'à 3 μm et longueur ≥ 30 μm).

2. On n'observe pas de film amorphe intergranulaire dans le SiC à ténacité améliorée, tandis que, dans les matériaux en Si_3N_4, les joints de grains amorphes sont toujours détectés. Les observations au MEHR nous permettent de conclure que la présence ou l'absence de films intergranulaires amorphes gouvernent la résistance à la rupture et les mécanismes de renforcement en général.

1 Introduction

Monolithic ceramics have been investigated intensively due to their promising potential as high-temperature structural materials.[1-5] The increasing importance of these materials, especially the pronounced interest in non-oxide ceramics, is closely related to their favorable combination of mechanical, chemical and thermomechanical properties, hence favoring this material group over intermetallics or superalloys under extreme conditions. Especially their high fracture strengths, low thermal expansion coefficient, good oxidation behavior, thermal shock and wear resistance in combination with a low density make them particularly interesting for applications under severe service conditions.[6-12]

In contrast to the aforementioned advantageous and promising material properties the general *brittleness* of monolithic ceramics, i.e. low fracture toughness values, is a major concern for a variety of potential applications; a problem arising for *all* structural ceramic materials.[13-15] The requirements regarding wide application of structural ceramics are manifold: preparation as complex-shaped components, withstanding temperatures up to 1400°C, good oxidation and chemical resistance, high fracture strength *and* high fracture resistance, so that strength becomes less sensitive to the flaw size in the material, resulting in improved reliability. Therefore, many attempts have been made to improve the fracture toughness of ceramic materials. One of the most effective concepts for improving fracture resistance is the addition of a second reinforcing phase. The incorporation of a second phase into the monolithic ceramic matrix leads to the initiation of different fracture mechanisms during crack propagation, which may result in both increased fracture strength and improved fracture toughness of the composite. The interaction of different fracture mechanisms in particle-, platelet-, whisker- or fiber-reinforced composites was shown to result in a pseudo-plastic shape of the stress–strain curve, although crack propagation on the submicron scale is still considered to be brittle.[16-22] Silicon carbide has been widely used as a reinforcing phase due to its favorable combinations of properties, including high strength, high elastic moduli and good thermal stability. Furthermore, its compatibility with most oxide and non-oxide ceramic materials led to the formation of a large variety of new ceramic composite materials with improved mechanical properties such as nanocomposites with their excellent high-temperature properties.[23] However, the reported data, e.g. for Si_3N_4/SiC whisker-reinforced ceramics, are not as promising as expected and even detrimental in some cases, due to difficulties in processing, thermal stability of the reinforcement, or interface structure.[24-27]

As most non-oxide ceramics cannot be conventionally densified via classical solid-state sintering techniques, liquid-phase sintering is commonly applied to fully densify the materials. The requirement of a liquid phase during pressureless or gas-pressure sintering is due to the high covalent bonding character and the low self diffusivity of the non-oxide materials.[28-30] Moreover, the densification process of composite materials with a high amount of reinforcing phase is a very complex and critical parameter. In general, an even higher amount of secondary liquid phase in conjunction with sophisticated processing techniques are required to completely densify these materials, because the addition of platelets or whiskers hinders densification. The relatively low density and high secondary-phase content are responsible for the detrimental effects on mechanical properties at elevated temperatures, which applies to most composite materials. Therefore, to avoid the problems associated with composite materials, while

taking advantage of their improved fracture resistance, new concepts have been developed to reinforce monolithic ceramics *in situ*, e.g. in-situ reinforced Si_3N_4 materials.[31-34]

This paper investigates the microstructural evolution of liquid-phase sintered SiC and Si_3N_4 materials by means of transmission electron microscopy (TEM). The aim of the study is to correlate observed microstructural features of these monolithic, non-oxide ceramics to improved fracture toughness. This includes the characterization of crystalline secondary phases formed upon densification as well as the structure and chemistry of homophase and heterophase boundaries. Toughness of ceramic materials as well as of composites is mainly governed by the mechanical behavior of the interface between adjacent particles. For example, in the bridging-zone model debonding of the reinforcing grains along the interface plays an essential role.[35-38] Thus, as the two major toughening mechanisms for structural ceramics are the bridging-zone and process-zone mechanisms, the characteristics of the grain- and phase-boundary structure are believed to play an important role in the performance of these ceramic materials and their resulting fracture toughness. A correlation between the measured fracture resistance and the observed interface structure will be presented.

2 Experimental Procedure

The SiC materials investigated were processed via liquid-phase sintering of α-SiC starting powders utilizing Y_2O_3 plus Al_2O_3 or AlN as sintering aids. All samples were pressureless sintered in a graphite resistance furnace under N_2 atmosphere. Post-HIPing in argon assured nearly complete densification of the specimens. The Si_3N_4 materials were processed via the RBSN route. Si powder fluxed with different rare-earth and transition-element oxides such as Y_2O_3, Sc_2O_3, and Nd_2O_3 were nitrided and subsequently densified utilizing a two-step gas-pressure sintering cycle with increased N_2 pressure.

The evaluation of the fracture toughness of the SiC and Si_3N_4 materials has been conducted using a flexural method based on a precracked chevron notch. The chevron notch configuration includes a small surface segment retained at the apex of the chevron. A Knoop indentation, using a Knoop indentor and a 100 N load, is placed at the apex to introduce a sharp precrack. The specimens were tested in three-point flexure with load/displacement (P/d) records monitored on the specimens during each test. Validity of the test is assessed from the non-linearity of the P/d curve preceding the peak load, requiring that stable crack extensions precede rupture and hence that the displacements are non-linear. Using the technique mentioned, fracture toughness data for several SiC and Si_3N_4 materials are summarized in Table 1. It is important to note that the toughened SiC material showed about twice the toughness of commercial SiC grades and that it is also tougher than a commercial Si_3N_4. Moreover, the Si_3N_4 materials displayed a two- to threefold increase in fracture toughness compared to commercially available Si_3N_4 grades.

Table 1. Fracture toughness results ($MPa\sqrt{m}$)

Material	*Chevron notch*
Commercial SiC	$2{\cdot}5 \pm 0{\cdot}5$
Toughened SiC	$6{\cdot}5 \pm 0{\cdot}5$
Commercial Si_3N_4	$4{\cdot}5 \pm 0{\cdot}5$
Toughened Si_3N_4[a]	$10 \pm 1{\cdot}0$

[a] This Si_3N_4 has about 20% by volume of large elongated grains.

The overall microstructure of the monolithic ceramic materials has been characterized by conventional transmission electron microscopy (CTEM). Qualitative phase analysis from bulk materials was determined by standard X-ray diffraction (XRD) techniques. Investigation of the characteristic microstructural and interfacial features was performed by high-resolution electron microscopy (HREM) utilizing a Joel 4000 EX operating at 400 kV. Analytical electron microscopy involved small probe microanalysis (EDS, ELS) and convergent beam electron diffraction (CBED). Transparent TEM foils of the different materials were prepared by standard ceramographic techniques involving grinding, dimpling, ion-beam thinning to perforation and light carbon coating to reduce electrostatic charging in the microscope.

3 Results and Discussion

3.1 Characterization of the SiC materials

The monolithic SiC ceramic with increased fracture resistance typically showed a homogeneous grain size of about 1–2 μm in diameter. The SiC particles revealed a more globular morphology compared to the Si_3N_4 materials, described later. The SiC grains often consisted of multiple polytypes. Both XRD and electron diffraction identified the SiC grains as an intergrowth of the 6H and 4H SiC polytypes with 6H being the predominant phase. A common occurrence is the bisection of single SiC grains by an

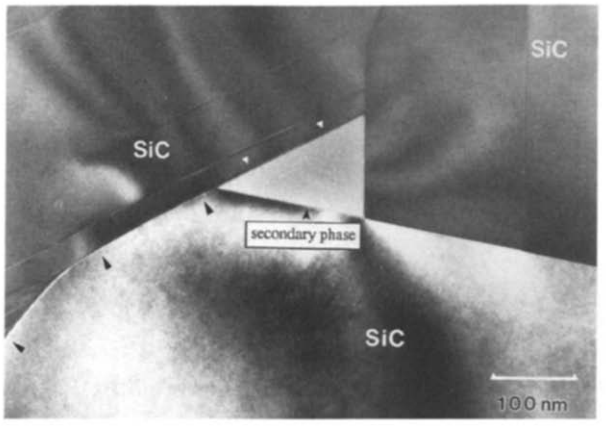

Fig. 1. Triple-grain region of the SiC material with improved fracture toughness. The secondary phase pocket is completely crystalline with no residual amorphous material left at the tip of the grain junctions (compare to Fig. 6). Note the sharp triangular shape of the secondary-phase pocket (poor wetting).

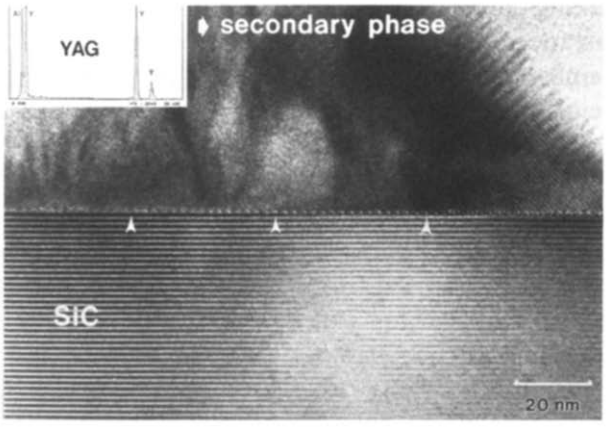

Fig. 2. Heterophase boundary in SiC (improved toughness) revealing periodic contrast changes along the interface, which are thought to be due to misfit dislocations at the boundary (thermal expansion mismatch between SiC and YAG, see EDS inset). No amorphous intergranular film is present at the heterophase boundary.

interface between 4H and 6H polytypes, as evident from electron diffraction patterns. Many of the matrix grains revealed a high dislocation density which can be related to the post-hipping procedure during processing. Apart from SiC particles, crystalline secondary phases are present at triple-point junctions. AEM in combination with CBED, EDS and ELS studies identified the secondary phase as YAG in most cases (Y–Al garnet, $Y_3Al_5O_{12}$) with a volume fraction of approximately $f = 0{\cdot}10$–$0{\cdot}15$ (estimated by TEM). It is important to note that the triple-grain regions were completely crystalline with *no* residual amorphous material left at the tip of these three-grain junctions (Fig. 1). Such residual glass pockets are a common feature for all Si_3N_4 materials (compare to Fig. 6). The complete crystallinity in conjunction with the sharp triangular shape of the secondary-phase pockets suggests poor wetting behavior of the secondary phase during liquid-phase sintering.

Additional HREM studies were performed to characterize the phase-boundary structure. No residual amorphous secondary phase was present at the secondary phase/SiC heterophase boundaries. The absence of a thin amorphous intergranular film along the phase boundaries, commonly observed in liquid-phase sintered ceramics, is vividly demonstrated by the observation of periodic contrast changes along the interface (Fig. 2). These contrast variations are believed to be due to the occurrence of misfit dislocations along the boundary due to the high thermal expansion mismatch of SiC and secondary phase. The strain fringes occur only in association with the second phase; they have yet to be quantified, as they have an important implication on fracture toughness and on the toughening mechanism. Furthermore, no residual amorphous phases could be detected at the SiC/SiC interfaces. The SiC grain boundaries were more difficult to examine due to the globular morphology of the particles. However, those techniques that usually allow amorphous phases to be unequivocally identified gave no evidence of such amorphous intergranular films along the boundaries. The applied techniques included high-resolution lattice imaging, diffuse dark-field imaging, and the Fresnel fringe technique.[39–41]

Various experimental procedures have been implemented to study the relevant toughening mechanism. Firstly, TEM studies have been conducted on thin foils that include cracks produced using a special processing technique described elsewhere in detail.[42] An array of hardness indentation is used to introduce cracks and a thin foil is prepared at the convergence of these cracks. Secondly, profilometer traces have been made across cracks in polished surfaces of bulk material to ascertain the non-linear material behavior. The TEM studies indicate profuse microcracking in a zone around the primary crack and in the wake of the crack, suggestive of a microcrack toughening mechanism (see Fig. 3). Furthermore, the microcracks seemingly nucleate at the interface between the crystalline secondary YAG phase and the SiC matrix grains, and also extend across the neighboring SiC/SiC grain boundary. The profilometer measurements revealed a roughness induced by polishing of about 5 nm remote from the crack. However, traces across the crack revealed *excess* surface displacements over a total width of 40–50 μm with a maximum uplift of about 20 nm. A non-linear process zone having a width of 20–25 μm is thus implied.

The preceding results suggest that microcracking

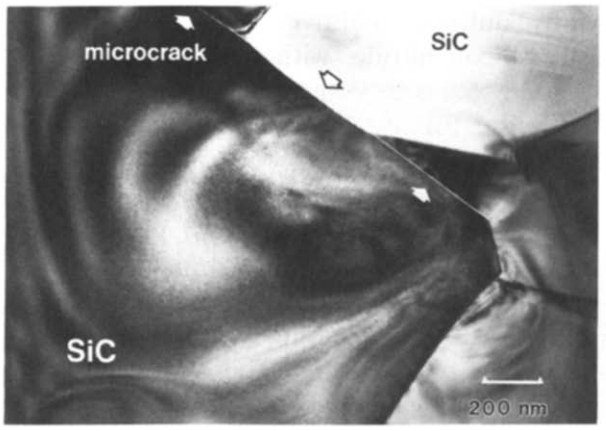

Fig. 3. Bright-field image of a thin foil including precracks produced by Vickers indentation. A microcrack running along the heterophase and homophase boundary is indicated by arrows. The microcracks seemingly nucleate at interfaces between secondary phase and SiC matrix grains.

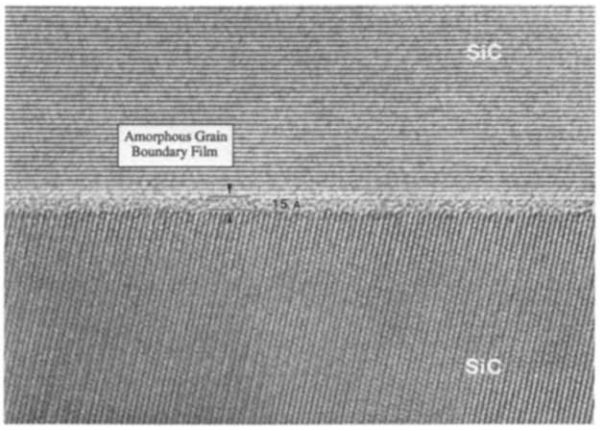

Fig. 4. HREM image of a SiC/SiC grain boundary. The amorphous intergranular film with a thickness of 15 Å is indicated. The occurrence of amorphous grain-boundary films in this material (low fracture toughness) is related to the additive composition used.

is the predominant toughening mechanism. The microcracks are seemingly induced by the residual strain associated with the secondary YAG phase and also cause dilatation within a process zone width of 20–25 μm. Microcrack toughening models, including the influence of the lower modulus of the microcrack process zone, and secondly the dilatation caused by relief of the local residual tension at the microcrack site, appropriate to these observations are elaborated elsewhere.[42]

Apart from theoretical considerations an experimental approach was considered to prove the importance of clean interfaces on improved fracture resistance in the SiC material already described. A SiC material was processed under identical processing conditions with the only difference being sintering-aid composition. In this case Al_2O_3 was used instead of AlN. For densification of Si_3N_4 materials the addition of $Y_2O_3 + Al_2O_3$ is commonly used, leading to completely densified grades; however, amorphous secondary phases are generally present at triple-grain junctions as well as along grain and phase boundaries. TEM and HREM investigations of the equivalent SiC material revealed residual amorphous phases present at both triple junctions and grain boundaries as well (Fig. 4). The occurrence of amorphous intergranular films in this material seemingly indicates that the secondary-phase composition completely wets the grain boundaries. The implication on fracture toughness is twofold: firstly, the crack path is purely intergranular and, secondly, *no* microcracks could be observed in this material. Moreover, the measured fracture resistance of this material is in the range of commercially available grades with $3{\cdot}0 \pm 0{\cdot}5\,\mathrm{MPa}\sqrt{\mathrm{m}}$. The results demonstrate that a clean interface structure, and the absence of amorphous grain- and phase-boundary films, has a marked influence on the resulting fracture toughness and the governing toughening mechanism. It can be concluded that the formation of an amorphous grain-boundary film supports the release of residual strain at the interface which can arise along heterophase boundaries due to high thermal expansion mismatch. Therefore, the observation of microcracks in the crack tip region of the toughened SiC is closely related to the interface structure (clean phase boundaries) and hence the predominant toughening mechanism in this material is microcrack toughening.

3.2 Characterization of the Si_3N_4 materials

The Si_3N_4 materials investigated in this study contained different additive compositions. Unexpectedly, the general microstructures of all materials as well as the resulting fracture toughness were nearly identical. Compared to the SiC materials described in the previous section, the Si_3N_4 grades are characterized by large, elongated β-Si_3N_4 grains embedded in a fine-grained Si_3N_4 matrix (Fig. 5). The diameter of these large grains was up to 3 μm and the particle length $\geq 30\,\mu$m. The volume fraction of the elongated Si_3N_4 grains was estimated by SEM (polished and plasma-etched surfaces) and TEM to be approximately $f = 0{\cdot}20$–$0{\cdot}25$. Regarding the growth mechanism of these large particles it is thought that β-Si_3N_4 nuclei, formed at an early stage of densification, continuously grow during liquid-phase sintering, resulting in the observed exaggerated grain growth.[43]

During sintering the rare-earth or transition-element oxide additives used as sintering aids will

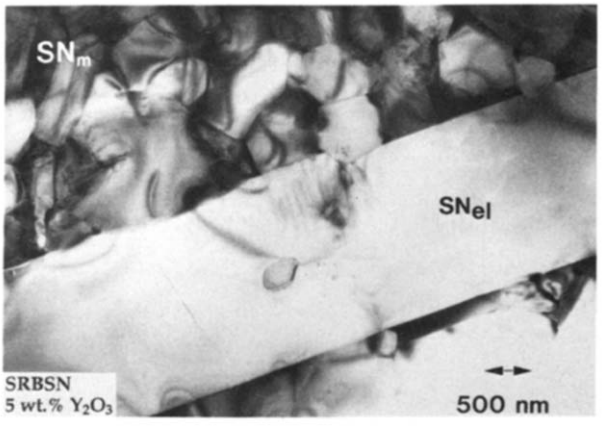

Fig. 5. Bright-field image of the Si_3N_4 material fluxed with 5 wt% Y_2O_3. Large, elongated β-Si_3N_4 grains (SN_{el}) with a diameter of up to 3 μm and a length of ≥ 30 μm are embedded in a fine-grained Si_3N_4 matrix (SN_m).

react with SiO_2, which is always present on the Si_3N_4 particle surfaces, and form a liquid that allows densification of the green body to near theoretical density.[44-46] This densification process resulted in the observed microstructure consisting of large β-Si_3N_4 grains (up to a few μm in diameter) embedded in a fine-grained matrix *and* a small percentage of secondary phases. The secondary phases are generally present in both three- and four-grain junctions of the matrix grains and along the interface of two matrix grains or at heterophase boundaries. It is well established that the presence of such secondary phases limits the high-temperature properties of non-oxide ceramic materials.[47-50] This is closely related to the properties of the secondary phases such as thermal stability and oxidation resistance. After densification the secondary phases are usually amorphous. However, a post-sintering heat treatment or a controlled sintering cycle can promote crystallization of these phases. Many attempts have been made to crystallize the secondary phases and thereby reduce the amount of amorphous phase present in the ceramics, in order to improve high-temperature mechanical properties. In some cases the crystallization of the secondary phase showed slight improvements to the high-temperature properties, but in most cases it was not found to be beneficial, especially for fracture strength data measured at room temperature.[51,52] This has been attributed to a higher concentration of impurities in the remaining amorphous intergranular phase. Moreover, internal stresses induced in the ceramic material due to volume changes upon phase transformation or to thermal expansion mismatch between matrix material and crystallized secondary phase can induce a degradation of the mechanical properties.

Many different additives have been used to densify silicon nitride, with mainly three factors influencing the selection of the sintering aid: (i) sinterability; (ii) refractoriness of the secondary phases; and (iii) crystallization of the triple-point pockets.[53-55] The most common additives used for liquid-phase sintering of Si_3N_4 are $Y_2O_3 + Al_2O_3$ which satisfy the first requirement, but it is difficult to obtain complete crystallization of the secondary-phase pockets.[56-58] It should be pointed out that the term 'complete crystallization' is used here with the understanding that the aforementioned triple-grain pockets are crystallized into the tip of the corners with no residual glass left (see also Figs 1 and 6). In Si_3N_4 ceramics it is possible to crystallize the triple-point regions but all the attempts to devitrify the amorphous material along homo- and hetero-phase boundaries have failed. Thin amorphous intergranular films are observed between *all* but low-angle or special grain boundaries.[59] They are generally assumed to consist of cations of the sintering aids and SiO_2 from the particle surfaces of the matrix grains, although a quantitative chemical analysis of these films has not yet been accomplished, due to both interference with adjacent grains and beam broadening, especially in amorphous materials, during chemical analysis in the electron microscope. Recent results have shown the presence of excess oxygen and rare-earth cations in the grain-boundary films.[60-62] The idea that the formation of an amorphous intergranular film in ceramics is an equilibrium phenomenon was first explored by Clarke.[63] He considered attractive and repulsive forces acting on the adjacent grains across the intergranular film and was able to derive a formula which allows, in theory, the calculation of

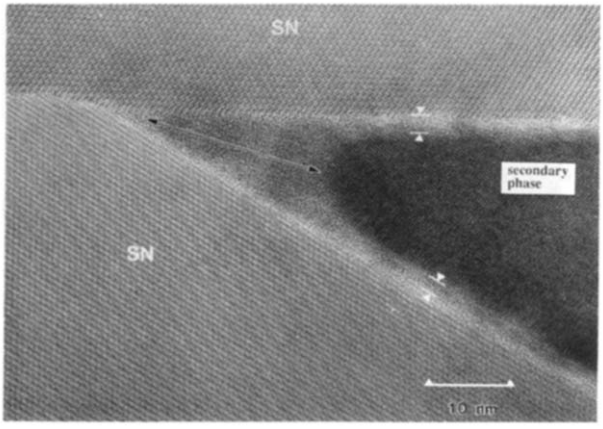

Fig. 6. HREM image of a triple-grain junction in the Si_3N_4 material. Note the rounded tip of the crystalline secondary phase and the residual amorphous material left at the corner of the pocket (arrow). The amorphous intergranular films covering the secondary phase are also indicated.

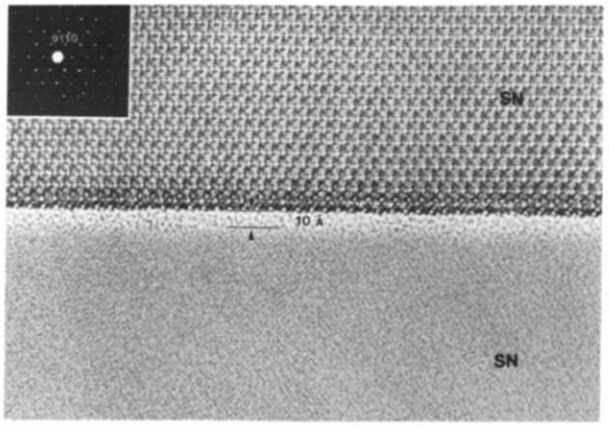

Fig. 7. HREM image of an amorphous intergranular film along the Si_3N_4/Si_3N_4 grain boundary. The upper grain is oriented along the [0001] direction (see inset of corresponding electron diffraction pattern). The grain-boundary film width of 10 Å is indicated.

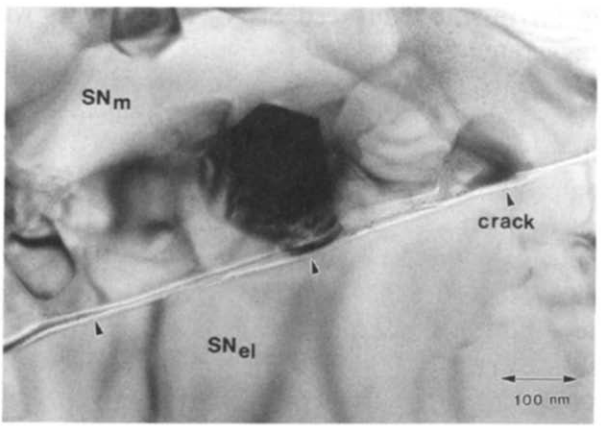

Fig. 8. Bright-field image depicting a crack running along the interface of an elongated Si_3N_4 grain (SN_{el}) and the fine-grained Si_3N_4 matrix (SN_m). It is assumed that debonding occurs along the thin amorphous grain-boundary layer (see also Fig. 7).

the equilibrium grain-boundary film thickness. However, some of the parameters involved in the derived equation are still unknown and difficult to obtain, e.g. the dielectric and elastic constants of the secondary phase. Therefore, HREM was used to image grain-boundary films in Si_3N_4 materials and to determine the corresponding film width.[60-62,64] Generally, all Si_3N_4 materials investigated showed a thin amorphous grain-boundary film covering the particles, independent of additive composition (see Fig. 7). The film was present at Si_3N_4/Si_3N_4 grain boundaries as well as at secondary phase/Si_3N_4 phase boundaries. It is important to note that heterophase boundaries always reveal a larger width of the amorphous interlayer compared to homophase boundaries, which is consistent with the theory on equilibrium film thickness. Moreover, the greater thickness of heterophase-boundary films favors relaxation of residual strain which mainly occurs along secondary phase/matrix interfaces (thermal expansion mismatch).

The substantially higher toughness of these materials has been attributed to both the order of magnitude larger reinforcement size of the in-situ grown large β-Si_3N_4 grains compared with SiC whisker-reinforced materials *and* to the occurrence of amorphous intergranular films which enable debonding. This scaling of toughness with reinforcement size is consistent with the toughening governed by the debonding and sliding of reinforcements with high aspect ratio.[65-67] A necessary prerequisite for the bridging-zone mechanism is a relatively weak interface structure to support *debonding*. It is assumed that debonding occurs along the thin amorphous grain-boundary layer between the elongated grains and the matrix (Fig. 8). Therefore, the occurrence of amorphous intergranular films along grain and phase boundaries supports debonding along the interface and hence governs the toughening mechanism of crack bridging for in-situ reinforced Si_3N_4 components revealing exaggerated grain growth.

4 Summary

The results show that in SiC materials a clean interface, in particular the absence of amorphous grain- and phase-boundary films, has a marked influence on the resulting fracture resistance and the governing toughening mechanism. Moreover, it can be concluded that the formation of amorphous grain-boundary films is ruled by the additive composition. The occurrence of intergranular films supports the release of residual stresses at the interface, which can arise along heterophase boundaries due to high thermal expansion mismatch. The fact that heterophase boundaries show a larger film width favors stress relaxation. Therefore, the observation of microcracks in the crack tip region is closely related to the interface structure, to clean phase boundaries. Hence, the predominant toughening mechanism in the SiC material with improved fracture resistance is microcrack toughening.

All Si_3N_4 materials investigated revealed, independent from additive composition, a nearly identical overall microstructure: (i) large, elongated Si_3N_4 grains embedded in a fine-grained matrix; and (ii) occurrence of amorphous homophase- and heterophase-boundary films. The presence of amorphous intergranular films covering all interfaces supports debonding along the interface and hence governs the toughening mechanism of crack bridg-

ing for in-situ reinforced Si_3N_4 components with exaggerated grain growth.

The study of two monolithic non-oxide ceramics gave clear evidence that the formation of amorphous intergranular films is closely related to the chemical composition of secondary phases formed during sintering. Moreover, the presence (or absence) of amorphous grain-boundary films affects the mechanical properties of the interfaces and hence governs the resulting *toughening mechanism*. Therefore, a careful control of the overall chemistry in conjunction with detailed analytical electron microscopy studies is an ongoing effort.

Acknowledgements

The author is grateful to Dr W. Braue and Dr M. K. Cinibulk for many helpful discussions. Moreover, the author would like to thank the BMFT for support under the contract number NTS 0230/0.

References

1. Prochazka, S., Sintering of silicon carbide. In *Proc. of the Conference on Ceramics for High Performance Applications*, Hyannis, MA, 1973, ed. J. J. Burke, A. E. Gorum & R. M. Katz. Brook Hill, Chestnut Hill Publ. Co., MA, USA, 1974, pp. 239–52.
2. Anderson, C. A. & Bratton, R. J., Ceramic materials for high temperature turbines. Final Report, ERDA, Washington, DC, AC-05-760-90405, 1977.
3. Coppola, J. A., Hailey, L. N. & McMurtry, C. H., Process for producing sintered silicon carbide ceramic body. US Patent 4 124 667, 7 November 1978.
4. Burke, J. J., Lenoe, E. N. & Katz, R. N., *Ceramics for High Performance Applications*, I (1974), II (1977), III (1980). Brook Hill Publ. Co., Chestnut Hill, MA, USA.
5. Riley, F. L., Progress in nitrogen ceramics. In *Proc. of NATO Advanced Study Institute on Nitrogen Ceramics*, Brighton, 1981. Martinus Nijhoff Publ., 1983.
6. Thümmler, F., Sintering and high-temperature properties of Si_3N_4 and SiC. In *Sintering Processes*, ed. G. C. Kuczynski. Plenum Publ. Corp., 1980, pp. 247–77.
7. Prochazka, S., The sintering process for SiC: a review. Techn. Report 81-CRD-314, General Electric Co., Schenactedy, NY, 1981.
8. Govila, R. K., Strength characterization of yttria-doped sintered silicon nitride. *J. Mater. Sci.*, **20** (1985) 4345.
9. Ziegler, G., Heinrich, J. & Wötting, G., Review: Relationships between processing, microstructure and properties of dense and reaction-bonded silicon nitride. *J. Mater. Sci.*, **22** (1987) 3041–86.
10. Bonnell, D. A., Structure of grain boundary phases in silicon nitride. *Mater. Sci. Forum*, **47** (1989) 132–42.
11. Ekström, T., Falk, L. K. L. & Knutson-Wedel, E. M., Pressureless-sintered Si_3N_4–ZrO_2 composites with Al_2O_3 additions. *J. Mater. Sci. Lett.*, **9** (1990) 823–6.
12. Komoda, H. & Miyoshi, T., Study of fracture behavior of very fine-grained silicon carbide ceramics. *J. Am. Ceram. Soc.*, **73** (1990) 3081–6.
13. Terwilliger, G. R., Properties of sintered silicon nitride. *J. Am. Ceram. Soc.*, **57** (1974) 48–9.
14. Niihara, K., Mechanical properties of chemically vapor deposited nonoxide ceramics. *Am. Ceram. Soc. Bull.*, **63** (1984) 1160–4.
15. Dutta, S., Densification and properties of α-silicon carbide. *J. Am. Ceram. Soc.*, **73** (1985) C-269.
16. Becher, P. F. & Wei, G. C., Toughening behaviour in SiC-whisker-reinforced alumina. *J. Am. Ceram. Soc.*, **67** (1984) C-267–C-269.
17. Wei, G. C. & Becher, P. F., Development of SiC-whisker reinforced ceramics. *Am. Ceram. Soc. Bull.*, **64** (1985) 298–304.
18. Hori, S., Yoshimura, M. & Somia, S., Strength–toughness relations in sintered and isostatically hot-pressed ZrO_2-toughened Al_2O_3. *J. Am. Ceram. Soc.*, **69** (1986) 169–72.
19. Kellett, B. J. & Lange, F. F., Hot forging characteristics of fine-grained ZrO_2 and Al_2O_3/ZrO_2 ceramics. *J. Am. Ceram. Soc.*, **69** (1986) C-172–C-173.
20. Rühle, M., Dalgleish, B. J. & Evans, A. G., On the toughening of ceramics by whiskers. *Scr. Metall.*, **21** (1987) 681–6.
21. Campbell, G. H., Rühle, M., Dalgleish, B. J. & Evans, A. G., Whisker toughening: A comparison between aluminium oxide and silicon nitride toughened with silicon carbide. *J. Am. Ceram. Soc.*, **73** (1990) 521–30.
22. Braue, W., Carpenter, R. W. & Smith, D. J., High-resolution interface analysis of SiC-whisker-reinforced Si_3N_4 and Al_2O_3 ceramic matrix composites. *J. Mater. Sci.*, **25** (1990) 2949–57.
23. Niihara, K., Suganuma, K., Nakahira, A. & Izaki, K., Interfaces in Si_3N_4–SiC nanocomposites. *J. Mater. Sci. Lett.*, **9** (1990) 598–9.
24. Greskovich, C. & Palm, J. A., Observations on fracture toughness of β-Si_3N_4–β-SiC composites. *J. Am. Ceram. Soc.*, **63** (1980) 597–601.
25. Tanaka, H., Greil, P. & Petzow, G., Sintering and strength of silicon nitride–silicon carbide composites. *Int. J. High Technol. Ceram.*, **1** (1985) 107–18.
26. Buljan, S., Baldoni, J. & Huckabee, M. L., Si_3N_4–SiC composites. *J. Am. Ceram. Soc.*, **60** (1987) 347–52.
27. Kleebe, H.-J., Corbin, N., Willkens, C. & Rühle, M., Transmission electron microscopy studies of silicon nitride/silicon carbide interfaces. *Mat. Res. Soc. Symp. Proc.*, **170** (1990) 79–84.
28. Kijima, K. & Shirasaki, S., Nitrogen self-diffusion in silicon nitride. *J. Chem. Phys.*, **65** (1976) 2668–71.
29. Mitomo, M., Tsutsumi, M., Bannai, E. & Tanaka, T., Sintering of silicon nitride. *Am. Ceram. Soc. Bull.*, **55** (1976) 313.
30. Greskovich, C. D., Prochazka, S. & Rosolowski, J. H., Sintering behavior of covalently bonded materials. In *Nitrogen Ceramics*, ed. F. L. Riley. Nordhoff, Leyden, 1977, pp. 351–7.
31. Claussen, N. & Jahn, J., Mechanical properties of sintered in-situ reacted mullite–zirconia composites. *J. Am. Ceram. Soc.*, **63** (1980) 228–9.
32. Tani, E., Nishijima, M., Ichinose, H., Kishi, K. & Umebayashi, S., Gas-pressure sintering of silicon nitride with an oxide addition. *Yogyo-Kyokai-Shi*, **94** (1986) 300–5.
33. Tani, T. & Wada, S, SiC matrix composites reinforced with internally synthesized TiB_2. *J. Mater. Sci.*, **25** (1990) 157–60.
34. Kleebe, H.-J. & Evans, A. G., The microstructure and toughness of in-situ reinforced silicon nitride. *J. Am. Ceram. Soc.*, 1991.
35. Charalambides, P. G. & Evans, A. G., Debonding properties of residually stressed brittle-matrix composites. *J. Am. Ceram. Soc.*, **72** (1989) 746–53.
36. Evans, A. G., Perspective on the development of high-toughness ceramics. *J. Am. Ceram. Soc.*, **73** (1990) 187–206.

37. Rühle, M., Evans, A. G., McMeeking, R. M., Charalambides, P. G. & Hutchinson, J. W., Microcrack toughening in alumina/zirconia. *Acta Metall.*, **35** (1987) 2701–10.
38. Evans, A. G. & Faber, K. T., Crack-growth resistance of microcracking brittle materials. *J. Am. Ceram. Soc.*, **67** (1984) 255–60.
39. Clarke, D. R., On the detection of thin intergranular films by electron microscopy. *Ultramicroscopy*, **4** (1979) 33–44.
40. Ness, J. N., Stobbs, W. M. & Page, T. F., A TEM diffraction-based method for characterizing thin grain-boundary and interfacial films. *Phil. Mag. A*, **54** (1986) 679–702.
41. Krivanek, O. L., Shaw, T. M. & Thomas, G., Imaging of thin intergranular phases by high-resolution electron microscopy. *J. Appl. Phys.*, **50** (1979) 4223–7.
42. Kleebe, H.-J. & Evans, A. G., The microstructural and toughening characteristics of liquid-phase sintered SiC. *J. Am. Ceram. Soc.*, (1992).
43. Hoffmann, M. S., Dreßler, W. & Hampp, E., personal communication, 1992.
44. Terwilliger, G. R. & Lange, F. F., Pressureless sintering of silicon nitride powders. US Patent 3,992,497, 1976.
45. Giachello, A., Martinengo, P. C., Tommasini, G. & Popper, P., Sintering of silicon nitride in a powder bed. *J. Mater. Sci.*, **14** (1979) 2825–30.
46. Lange, F. F., Fabrication and properties of dense polyphase silicon nitride. *Am. Ceram. Soc. Bull.*, **62** (1983) 1369–74.
47. Tsuge, A., Nishida, K. & Komatsu, M., Effect of crystallizing the grain-boundary glass phase on the high-temperature strength of hot-pressed Si_3N_4 containing Y_2O_3. *J. Am. Ceram. Soc.*, **58** (1975) 323–6.
48. Raj, R. & Lange, F. F., Crystallization of small quantities of glass (or a liquid) segregated in grain boundaries. *Acta Met.*, **29** (1981) 1993–2000.
49. Clarke, D. R., Lange, F. F. & Schnittgrund, G. D., Strengthening of a sintered silicon nitride by post-fabrication heat treatment. *J. Am. Ceram. Soc.*, **65** (1982) C-51–C-52.
50. Pierce, L. A., Mieskowski, D. M. & Sanders, W. A., Effect of grain-boundary crystallization on the high-temperature strength of silicon nitride. *J. Mater. Sci.*, **21** (1986) 1345–8.
51. Bonnell, D. A., Tien, T. Y. & Rühle, M., Controlled crystallization of the amorphous phase in silicon nitride ceramics. *J. Am. Ceram. Soc.*, **70** (1987) 460–5.
52. Cinibulk, M. K., Thomas, G. & Johnson, S. M., Grain-boundary-phase crystallization and strength of silicon nitride sintered with a YSiAlON glass. *J. Am. Ceram. Soc.*, **73** (1990) 1606–12.
53. Clarke, D. R. & Thomas, G., Microstructure of yttria-fluxed hot-pressed silicon nitride. *J. Am. Ceram. Soc.*, **61** (1978) 114–18.
54. Loehman, R. E. & Rowcliffe, D. J., Sintering of Si_3N_4–Y_2O_3–Al_2O_3. *J. Am. Ceram. Soc.*, **6** (1980) 144–8.
55. Hirosaki, N., Okada, A. & Matoba, K., Sintering of Si_3N_4 with the addition of rare-earth oxides. *J. Am. Ceram. Soc.*, **71** (1988) C-144–C-147.
56. Sanders, W. A. & Mieskowski, D. M., Strength and microstructure of sintered Si_3N_4 with rare-earth-oxide additions. *J. Am. Ceram. Soc.*, **64** (1985) 304–9.
57. Falk, L. K. L. & Dunlop, G., Crystallization of the glassy phase in an Si_3N_4 material by post-sintering heat treatments. *J. Mater. Sci.*, **22** (1987) 4369–76.
58. Cinibulk, M. K., Thomas, G. & Johnson, S. M., Fabrication and secondary-phase crystallization of rare-earth disilicate–silicon nitride ceramics. *J. Am. Ceram. Soc.*, (1992).
59. Schmid, H. & Rühle, M., Structure of special grain boundaries in SiAlON ceramics. *J. Mater. Sci.*, **19** (1984) 615–28.
60. Kleebe, H.-J., Cinibulk, M. K. & Rühle, M., TEM characterization of a ceria-fluxed silicon nitride. *J. Mater. Sci. Lett.*, (1991).
61. Vetrano, J. S., Kleebe, H.-J., Hampp, E., Hoffmann, M. J. & Cannon, R. M., Epitaxial deposition of silicon nitride during post-sintering heat treatment. *J. Mater. Sci. Lett.*, (1991).
62. Kleebe, H.-J., Vetrano, J. S., Bruley, J. & Rühle, M., TEM studies of grain boundary films in Si_3N_4 ceramics. In *Proc. 49th Annual EMSA Meeting*, 4–9 August 1991, San Jose, CA, USA, pp. 930–1.
63. Clarke, D. R., On the equilibrium thickness of intergranular glass phases in ceramic materials. *J. Am. Ceram. Soc.*, **70** (1987) 15–22.
64. Kleebe, H.-J., HREM study on grain-boundary film thickness in Si_3N_4 ceramics. In *Proc. 2nd Europ. Ceram. Conf.*, Augsburg, 11–14 Sept., 1991.
65. Tajima, Y., Urashima, K., Watanabe, M. & Matsuo, Y., Fracture toughness and microstructure evaluation of silicon nitride ceramics. In *Ceramic Transactions*, Vol. 1, *Ceramic Powder Science–IIB*, ed. G. L. Messing, E. R. Fuller & H. Haussner. Am. Ceram. Soc., Westerville, OH, 1988, pp. 1034–41.
66. Kawashima, T., Okamoto, H., Yamamoto, H. & Kitamura, A., Grain size dependence of the fracture toughness of silicon nitride ceramics. *J. Ceram. Soc. Japan*, **99** (1991) 320–3.
67. Becher, P. F., Microstructural design of toughened ceramics. *J. Am. Ceram. Soc.*, **74** (1991) 255–69.